MTLA 32 (2023) 101964

Contents lists available at ScienceDirect

Materialia

journal homepage: www.elsevier.com/locate/mtla

Full Length Article

Strain-induced clustering in Al alloys

Philip Aster [a,*], Phillip Dumitraschkewitz [b], Peter J. Uggowitzer [b], Florian Schmid [c], Georg Falkinger [c], Katharina Strobel [c], Peter Kutlesa [d], Michael Tkadletz [e], Stefan Pogatscher [a,*]

[a] Christian Doppler Laboratory for Advanced Aluminium Alloys, Chair of Nonferrous Metallurgy, Montanuniversitaet Leoben, Franz-Josef-Straße 18, Leoben 8700, Austria
[b] Chair of Nonferrous Metallurgy, Montanuniversitaet Leoben, Franz-Josef-Straße 18, Leoben 8700, Austria
[c] AMAG rolling GmbH, Lamprechtshausener Str. 61, Ranshofen 5282, Austria
[d] Erich Schmid Institute of Materials Science, Austrian Academy of Sciences, Jahnstr. 12, Leoben 8700, Austria
[e] Department of Materials Science, Montanuniversitaet Leoben, Franz-Josef-Straße 18, Leoben 8700, Austria

ARTICLE INFO

Keywords:
Aluminum alloys
Cluster hardening
Mechanical testing
Excess vacancies
Strain-induced clustering

ABSTRACT

Solute clusters represent the start of decomposition during aging of aluminum alloys and can generate strengthening while keeping the strain hardening high in comparison with shearable precipitates. In this study, clusters in a pre-aged AlMgSiCu 6xxx-series and a recently developed AlMgZnCu crossover alloy were investigated by atom probe tomography (APT) and tensile testing before and after straining. Pre-aging was performed at 100 °C and 60 °C respectively, and a tensile strain of 5% was applied. The key feature detected was the formation of clusters during plastic deformation, referred to here as "strain-induced clustering". It is explained based on diffusion enhancement by the strain-induced formation of excess vacancies during tensile testing, and evaluated by means of a simple modeling approach. In addition to the significant intrinsic contribution of clusters to strain hardening via dislocations, strain-induced clustering adds a hypothetical non-dislocation-based component to strain hardening.

Solute clusters are an age-hardening reaction [1–3] seen in all age-hardenable aluminum alloys. They can form at low ($\approx 0.3T_m$) to medium ($\approx 0.45T_m$) temperatures and can greatly influence material properties. Clusters are defined as a local accumulation of alloying atoms. They represent the first event in the precipitation sequence and thus generate the first hardening increment [4]. The starting point of clustering is a supersaturated solid solution (SSSS) after quenching that contains an excess of solute atoms without exhibiting a favorable energetic state. Local matrix strain due to atomic size or electronic differences to the host lattice act as driving forces for the aggregation of solute atoms. Diffusion processes, determined primarily by temperature, vacancy concentration, and lattice distortion, cause alloying solutes to migrate through the Al lattice [5,6]. Defects such as dislocations and excess vacancies resulting from plastic deformation can also have a considerable impact, significantly accelerating diffusion-controlled decomposition processes [7].

Another important aspect of clustering is the advantageous combination of strength and ductility found under certain conditions where clusters are present [8]. Deschamps et al. [9] suggested that the high strain hardening rates observed in as-quenched and naturally-aged Al-Zn-Mg alloys may result from the generation of new obstacles to dislocations during deformation. Dynamic precipitation has also been used to explain the homogeneity of deformation and high ductility [9]. Bignon et al. [10] integrated the excess vacancy formation upon deformation into a growth model to explore the deformation-precipitation linkage in a multicomponent aluminum alloy. In that context deformation generates an increase in the precipitation rate compared to static aging over an equivalent period [10]. Zhang et al. [11] systematically investigated the effects of solute clusters by using atom probe tomography (APT) to trace microstructure evolution during deformation in an Al-Zn-Mg alloy in T4 condition. They attribute the high level of strain hardening capability to a combination of clustering and a simultaneous reduction in stacking fault energy due to excess solute atoms in the Al matrix. The latter atoms interact with mobile dislocations and generate strain-enhanced diffusivity. As a result, high yield strengths, extensive strain hardening capacities and increased ductility can be achieved [11].

In this study we investigate the evolution of clusters upon deformation in a pre-aged AlMgSiCu of the 6xxx-series and in a novel

* Corresponding authors.
E-mail addresses: philip.aster@unileoben.ac.at (P. Aster), stefan.pogatscher@unileoben.ac.at (S. Pogatscher).

https://doi.org/10.1016/j.mtla.2023.101964
Received 24 July 2023; Accepted 11 November 2023
Available online 11 November 2023

AlMgZnCu crossover alloy [12], which both show pronounced strain hardening. APT measurements and a simple modeling approach revealed that significant cluster formation occurs simultaneously with plastic deformation, causing increased resistance to dislocation motion as a hypothetical component of strain hardening.

Table 1 shows details of the AlMgSiCu alloy (6xxx) and the AlMgZnCu crossover alloy (CA) investigated in the study. All alloys were produced at laboratory scale. The processing steps included a homogenization treatment and hot and cold rolling. The samples were solution treated in an air furnace at 540 °C for 20 min (6xxx) and 465 °C for 35 min (CA) and then water quenched to room temperature. A tensile test took place immediately after solution annealing and quenching; condition AQ (as-quenched) provides reference data on the mechanical properties of both alloy classes. Pre-aging (PA) at 100 °C/5 h (6xxx) and 60 °C/5 h (CA) was begun within 3 min of quenching. These treatments correspond to pre-aging treatments for these alloy types, and represent typical starting conditions for forming processes [3,8].

A Zwick/Roell BT1-FR100THW.A2K tensile testing machine equipped with a 50 kN load cell was used to evaluate mechanical properties. For each condition, three tensile specimens (manufactured according to EN ISO 6892–1) were mechanically tested at a strain rate of $3.2 \bullet 10^{-3}\, s^{-1}$.

Matchstick-shaped specimens of the APT samples in an undeformed state (approximately $0.7 \times 0.7 \times 20\ mm^3$) were prepared from the cold-rolled sheet by a combination of cutting and mechanical grinding and then subjected to the pre-aging treatment. This was immediately followed by a two-stage standard electropolishing process (1st stage: 25% HNO_3 in methanol; 2nd stage: 2% $HClO_4$ in 2-butoxyethanol) to minimize natural aging. After aging, some matchstick-shaped specimens were immediately strained to 5% plastic elongation using a special specimen holder and subsequently electropolished within 40 min, taking natural aging into account [13]. Where necessary, samples were transported in liquid nitrogen. APT experiments were performed within 12 h of electropolishing in voltage mode with a pulse fraction of 20%, a frequency of 200 kHz, and a detection rate of 1% at a temperature of 30 K on a LEAP 3000 X HR (6xxx) and on a LEAP 5000 XR (CA). The size of the APT datasets ranges from 12 to 30 million atoms. The formalism described by [8,13] and [3] was deployed for APT solute analysis and to evaluate the number density of detected clusters. The volumes of the APT reconstructions were measured using the built-in "AlphaShape" [14] function in MATLAB™. Alpha shapes were also used to identify the non-core atoms of each cluster, found by the maximum separation cluster search (IVAS 3.8.14) run with parameters based on the 10th NN (MgSiCu, 6xxx) and 5th NN (MgZnCu, CA) core atoms and using $d_{erode}=0$. The volume fraction was computed by the relation of the number of cluster atoms to the overall number of solute atoms in each APT specimen. The detection efficiency η equals 0.37 for the 6xxx alloy and 0.52 for the crossover alloy [15]. The composition of the solute clusters was extracted from cluster search data using customized scripts [16]. The corresponding error margin for number densities was calculated as described in [17]. Region of Interests (ROI) with a dimension of $20 \times 1 \times 50\ nm^3$ were chosen for a detailed representation of the cluster structure.

Fig. 1 displays the results of the tensile tests on the 6xxx-series alloy. The stress-strain curve reveals high levels of strain hardening and uniform elongation. Of specific interest, however, is the increased clustering observed after 5% strain. This is illustrated by the 3D element maps (ROI's, Fig. 1,c) and the APT number density evaluations (Fig. 1). Please note that the ROI's are 2D projections of 3D data. The dimension in y-direction corresponds to a length that avoids overlapping of clusters in the illustrations.

In Fig. 1d,e the number density of the MgSiCu-type solute atom clusters is plotted against the number of atoms, which reflects the size of the MgSiCu clusters. A high density of small clusters (10–25 atoms) and a decreasing number density at increasing cluster size is apparent in both strain conditions. In almost every size category, the number density in the 5% deformed state (striped gray bar) is significantly higher than in the undeformed state (solid gray bar). In summary, during 5% plastic deformation the number density of MgSiCu clusters increases by 38% in the range of 10–25 atoms, and by as much as 57% in the range of 26–50 atoms. One might now assume that the number density has been increased by the cutting processes of existing clusters. However, this is contradicted by the finding that plastic deformation also increases the volume fraction of the clusters, as shown in Table 2. Specifically, the volume fraction of all the clusters measured increases by roughly 50% in the deformed state compared to the undeformed state. Moreover, the fraction of solutes in clusters (see Table 2) is higher in the deformed state. According to the current findings, clusters seem to be generated during deformation.

The picture is similar for the crossover alloy after pre-aging. This alloy exhibits a high level of uniform elongation and pronounced strain hardening, despite the high yield stress around 275 MPa (see Fig. 2a).

In this alloy, too, the number density of the clusters increased significantly in the 5% strained sample (see Fig. 2b,c). An evaluation of the number density over the atoms contained in the clusters is given in Fig. 2d,e. In summary, the number density of MgZnCu clusters increases after 5% strain by 28% in the range of 5–10 atoms, and by as much as 41% in the range of 11–30 atoms.

Here the volume fraction of clusters also increases by about 20% compared to the undeformed state (Table 3). An analysis of the chemical composition of the MgZnCu clusters in the crossover alloy yields a picture like that of the 6xxx series, with a higher fraction of solutes in clusters in the deformed state.

Although commonly not addressed in standard room temperature tensile tests, strain-induced decomposition and phase transformation have been shown to occur in various Al alloys [7]. Several studies indicate that strain-induced excess vacancies play an essential role in this [18,19]. They are decisive for diffusion and enable decomposition and phase transformations even at comparatively low temperatures below 200 °C [9,18–22]. Studies of deformation at low to moderate temperatures revealed an excess vacancy concentration of up to 10^{-4}, which is orders of magnitude higher than the thermal equilibrium vacancy concentration [23,24]. This increase in vacancy concentration has significant implications for solute diffusion rates and is also considered crucial for strain-induced clustering.

According to Militzer et al. [25] and Robson [7], the evolution of the strain-induced excess vacancy concentration c_{ex} can be estimated by Eq. (1):

$$\frac{dc_{ex}}{dt} = \chi \frac{\sigma \Omega_0}{H_V^f} \dot{\varepsilon} - \frac{D_V \rho}{\kappa^2} c_{ex} \tag{1}$$

The first term on the right-hand side of the equation represents the generation of vacancies by plastic deformation, caused mainly by the non-conservative movement of dislocation jogs [7]. It contains the flow stress σ, the enthalpy of vacancy formation energy H_V^f, the atomic volume Ω_0, the plastic strain rate $\dot{\varepsilon}$ and a constant χ which determines the fraction of plastic work converted to vacancy formation. The second term represents the annihilation of vacancies at dislocations and comprises the vacancy diffusion constant D_V, the dislocation density ρ and a constant κ, which describes the geometric structure of the dislocation network. D_V is given by $D_V = D_V^0 \cdot exp(-H_V^m/RT)$, with the vacancy migration enthalpy H_V^m [7].

Table 1
Composition of the alloys under investigation.

Alloy	Elements, wt.-%						
	Mg	Zn	Si	Fe	Mn	Cu	Al
6xxx	0.9	0.0	0.4	0.2	0.1	1.0	Bal.
CA	5.0	3.8	0.1	0.2	0.4	0.8	Bal.

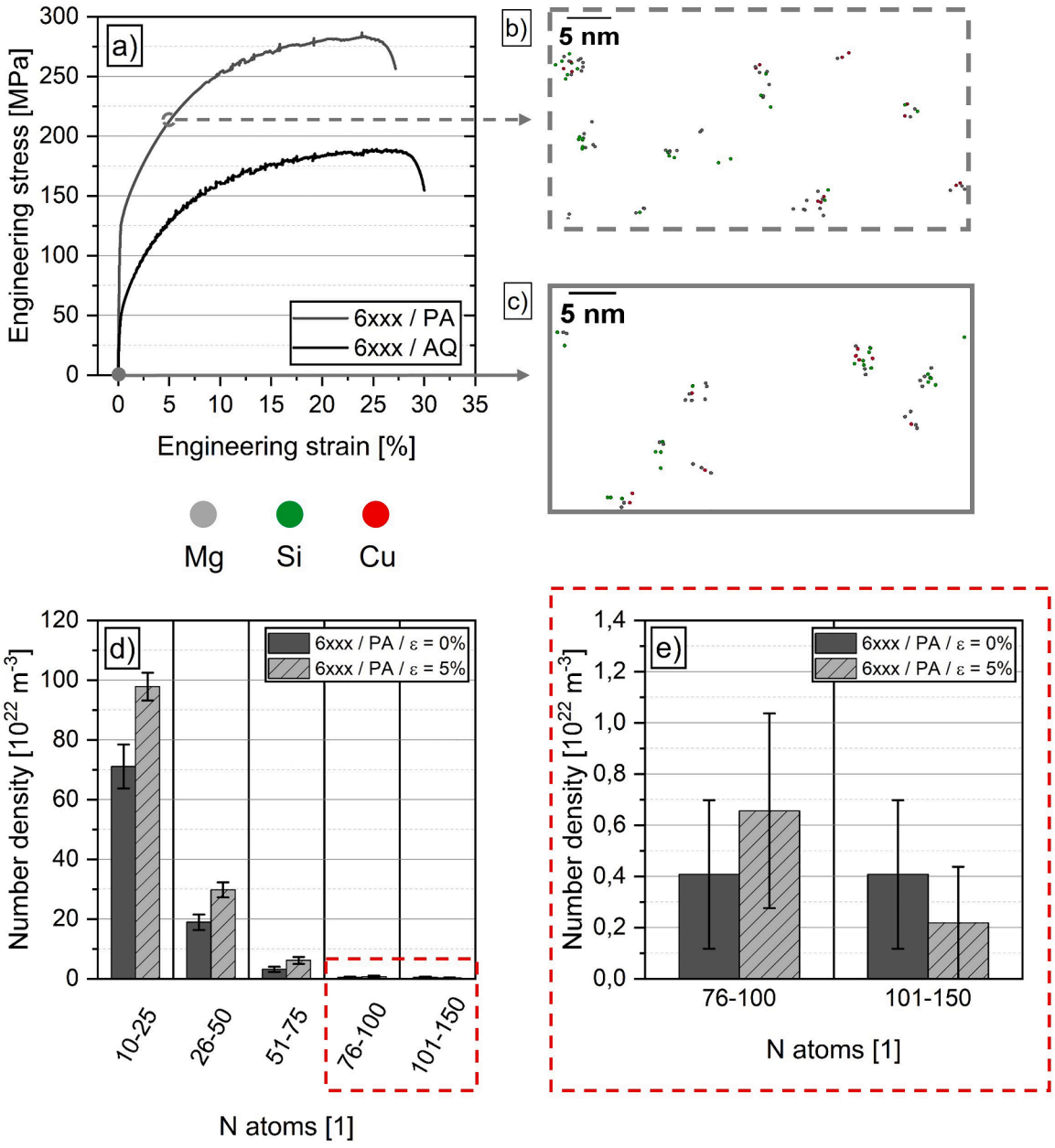

Fig. 1. Engineering stress-strain curve for the pre-aged and as-quenched 6xxx alloy (a); 3D elemental maps ($20 \times 1 \times 50$ nm^3) for MgSiCu clusters in the deformed (b) and undeformed (c) states; number density as a function of the atoms of the MgSiCu clusters in deformed (striped gray bar) and undeformed (solid gray bar) states (d); magnification view of the number density at larger numbers of atoms (e).

Table 2
Chemical analysis via APT of the pre-aged 6xxx alloy in different strain states.

Alloy	Strain [%]	Composition	Mg	Si	Cu
6xxx	0	Fraction of solutes in clusters (%)	6.7	9.0	5.4
		Rel volume fraction of clusters (%)		0.31	
	5	Fraction of solutes in clusters (%)	9.5	12.3	7.4
		Rel volume fraction of clusters (%)		0.47	

We extract the dislocation density from the flow stress σ from the experimentally recorded stress-strain curve utilizing the Taylor relation in Eq. (2):

$$\sigma - \sigma_0 = \alpha \cdot M \cdot G \cdot b \cdot \sqrt{\rho}, \tag{2}$$

where the initial yield stress σ_0 is subtracted from the flow stress to consider only the strain hardening contribution.

The concentration of vacancies c_0 generated during quenching from the solution annealing temperature and subsequent pre-aging treatment corresponds to the initial concentration in the undeformed state. In pure Al, the vacancy site fraction at temperature T is given by Eq. (3) [26,27].

$$c_0 = 2.3 \cdot exp\left(-\frac{H_V^f}{RT}\right) \tag{3}$$

We use the vacancy concentration at the pre-aging temperature. As described in [28], vacancies can be also trapped at higher temperatures, but because the calculation serves as an estimate to discuss the potential of strain-induced vacancy formation a conservative assumption may be appropriate.

Since Mg contributes significantly to cluster formation in both alloys, this alloying element was chosen to demonstrate the effect of strain-

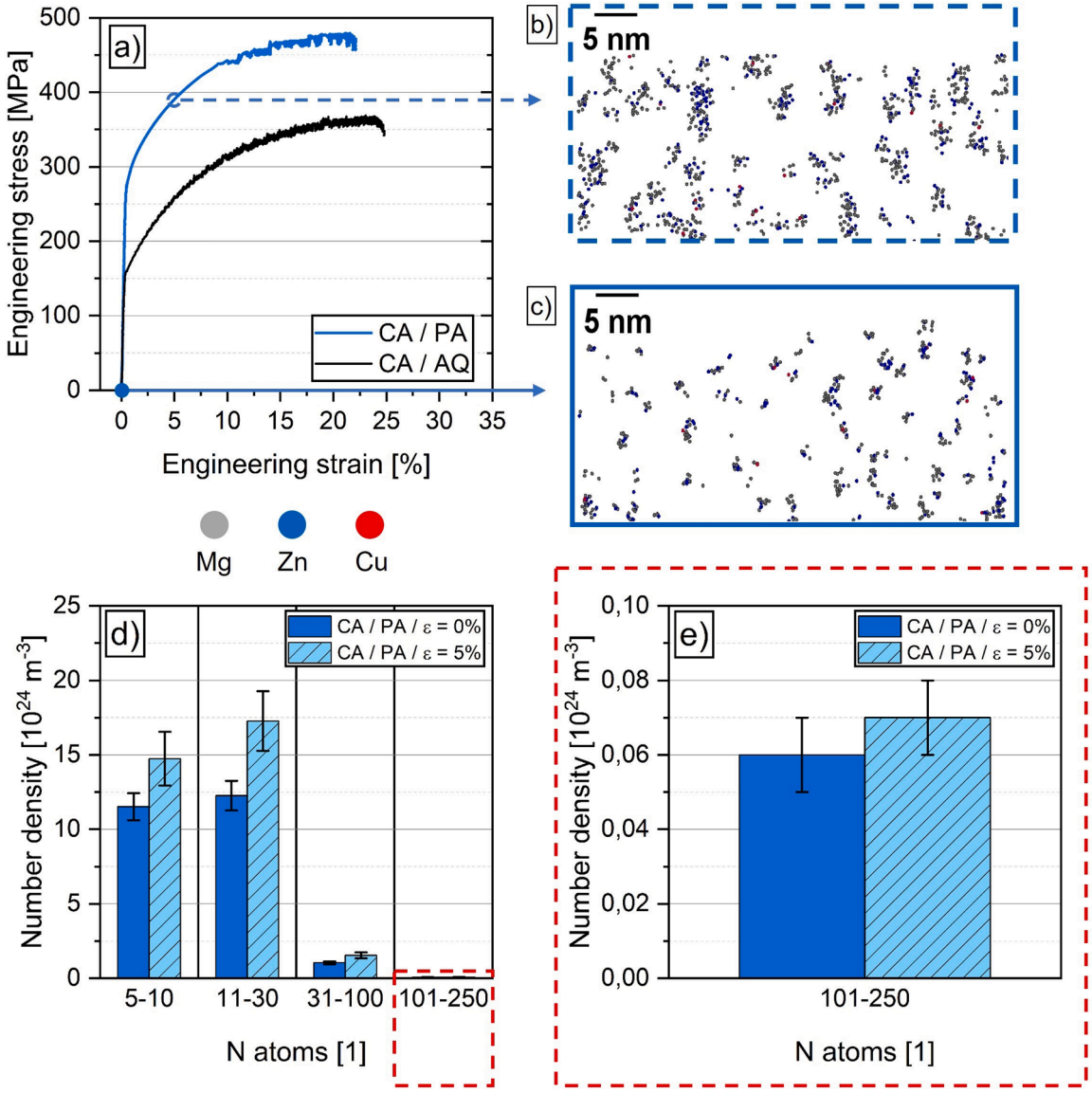

Fig. 2. Engineering stress-strain curve for the pre-aged and as-quenched crossover alloy (a); 3D elemental maps ($20 \times 1 \times 50$ nm^3) for MgZnCu-clusters in deformed (b) and undeformed (c) states; number density as a function of the atoms of the MgZnCu-clusters in deformed (striped blue bar) and undeformed (solid blue bar) (d); magnification view of the number density at larger numbers of atoms (e).

Table 3
APT chemical analysis of the pre-aged crossover alloy in different strain states.

Alloy	Strain [%]	Composition	Mg	Zn	Cu
CA	0	Fraction of solutes in clusters (%)	15.6	18.4	14.0
		Rel volume fraction of clusters (%)		1.66	
	5	Fraction of solutes in clusters (%)	19.2	21.9	18.2
		Rel volume fraction of clusters (%)		2.01	

induced vacancies on the diffusion length. The Mg diffusion length x_{Mg} after time t can be expressed by Eq. (4) [29].

$$x_{Mg}^2 = \int 4 \cdot f \cdot D_{Mg} \cdot dt \tag{4}$$

With the diffusion constant $D_{Mg} = D_{Mg}^0 \cdot \exp(-H_{Mg}^m/RT) \cdot \exp(-H_V^f/RT)$ and a diffusion enhancement factor $f = 1 + c_{ex}/c_0$ [7], Eq. (4) was solved iteratively with an explicit integration scheme.

Table 4 summarizes the model parameters used to estimate both the excess vacancy concentration and the diffusion length from a tensile test.

The results of the simulation are illustrated in Fig. 3, where the excess vacancy concentration (Fig. 3a) and the mean diffusion length of Mg (Fig. 3b) are plotted as a function of the true strain. At a strain of 5% (black dashed line) a high vacancy concentration on the order of 10^{-4} is present. The corresponding mean diffusion length of Mg reached during straining to 5% is around 5 nm.

It must be noted that the results of the model are influenced by the uncertainty of the parameters used, primarily the dislocation arrangement κ and the vacancy migration enthalpy H_V^m. An increase in κ above 1 (less homogeneous arrangement of dislocations) generates a higher excess vacancy concentration and thus an increased diffusion length. A reduction in H_V^m generates higher vacancy annihilation, which, however, has a significant effect on the diffusion length only at high plastic strains. At a strain of 5%, the diffusion length calculated by an "unfavorable" parameter variation (κ and H_V^m) is lower by a factor of 2 at the most. However, it should also be noted that the clustering that takes place during deformation also contributes to strain hardening, and accordingly needs to be taken into account in the model through a reduction in

Table 4
Model parameters and values used.

Parameter	Notation	Value	Reference/comment
Fraction of external work stored by producing vacancies	χ	0.1	0.01 to 0.1 [7,30]
Atomic volume	Ω_0	$1.66{\cdot}10^{-29}$ m^3	[7,19]
Vacancy / self-diffusion enthalpy	H_V^{sd}	129 kJ•mol^{-1}	[27]
Vacancy formation enthalpy	H_V^f	64 kJ•mol^{-1}	50 to 73 kJ•mol^{-1} [26,27,30–33]
Vacancy migration enthalpy	H_V^m	65 kJ•mol^{-1}	56 to 96 kJ•mol^{-1} [7,34]
Pre-factor vacancy diffusion	D_V^0	$3.0{\bullet}10^{-5}$ m^2•s^{-1}	(1 to 3)$\bullet10^{-5}$ m^2•s^{-1} [7,27]
Mg diffusion / Activation enthalpy	H_{Mg}^d	115 kJ•mol^{-1}	[35]
Pre-factor Mg diffusion	D_{Mg}^0	$6.2{\bullet}10^{-6}$ m^2•s^{-1}	[35]
Dislocation arrangement	κ	1.0	1 to 10 [25]
Gas constant	R	8.314 J•mol^{-1}•K^{-1}	[36]
Constant	α	0.3	
Taylor factor	M	3.06	[3,37]
Shear modulus	G	25.4 GPa	
Burgers vector	b	$0.286{\bullet}10^{-9}$ m	
Yield strength – AQ – 6xxx*	$R_{p0.2}^{AQ,\ 6xxx}$	53 MPa	
Yield strength – PA – 6xxx*	$R_{p0.2}^{PA,\ 6xxx}$	133 MPa	
Stress – PA-5% – 6xxx*	$\sigma_{PA-5\%}^{6xxx}$	225 MPa	
Yield strength – AQ – CA*	$R_{p0.2}^{AQ,\ CA}$	173 MPa	
Yield strength – PA – CA*	$R_{p0.2}^{PA,\ CA}$	283 MPa	
Stress – PA-5% – CA*	$\sigma_{PA-5\%}^{CA}$	413 MPa	Experimental
Matrix concentration – PA – 6xxx	$c_{MgSiCu}^{6xxx.PA}$	1.21 at.-%	
Matrix concentration – PA-5% – 6xxx	$c_{MgSiCu-5\%}^{6xxx.PA}$	1.03 at.-%	
Matrix concentration – PA – CA	$c_{MgZnCu}^{CA.PA}$	6.63 at.-%	
Matrix concentration – PA-5% – CA	$c_{MgZnCu-5\%}^{CA.PA}$	6.56 at.-%	

* corresponds to true stresses.

the dislocation hardening contribution. The contribution of cluster hardening (CH), solid solution hardening and strain hardening can be roughly estimated by using the relative volume fractions of the clusters (Table 2,3), the true yield strengths in the AQ, PA and PA-5% condition and concentration of solute atoms in the matrix (Table 4). We estimate the various contributions of the strengthening mechanisms by using Eq. (5):

$$\sigma = k_1\sqrt{c} + k_2\sqrt{\rho} + k_3\sqrt{f}, \tag{5}$$

where c represents the concentration of solute atoms in the matrix, ρ the dislocation density and f the volume fraction of the clusters. From Eq. (5) the dislocation density ρ in Eq. (1) is estimated. c and f are linearly estimated for a given strain valid as interpolation between the PA and PA-5 % values up to 5% strain and extrapolated beyond. With this, a higher vacancy annihilation and consequently a slightly lower diffusion length (shown by the gray and blue dashed lines in Fig. 3) is seen. However, the results demonstrate that the influence, at least at low strains, is negligible.

The spatial distribution of the clusters is important in considering their effect on dislocation motion. Therefore, the experimental inter-cluster distance distribution is determined by quantitative investigation of the 3D-data. For this purpose, the 1st nearest neighbor distance (1NN) of each cluster, defined by the Mg-based centroid, is being measured and normalized over the total volume of the respective APT dataset. The spatial distribution of both alloys in Fig. 4, either in the undeformed or in the deformed state, is shown to be homogeneous in a specific distance range. However, especially clusters with either a very small or a very large distance between each other make the cluster distribution in Figs. 1 and 2 appear rather heterogeneous. In the 6xxx series, the majority of clusters are found in a distance range of 4–6 nm (see Fig. 4a). Regarding the crossover alloy in Fig. 4b, clusters with a spacing of 1.2–2.0 nm dominate. According to the calculations in Fig. 3b, the diffusion length of Mg at 5% plastic deformation, is between 5 and 6 nm, depending on the alloy. Diffusion of Mg associated with excess vacancies results in the formation of new clusters. As a result, the cluster count is higher in the deformed state (see dashed lines in Fig. 4). A higher cluster number compared to the undeformed state, leads to a reduced distance between the clusters, which results in an increased resistance to the dislocation motion.

Note that in age-hardenable Al alloys, plastic deformation can be highly localized. As reported in [38], high strain localization can be expected to have a strong negative effect on ductility [38]. However, the high achieved fracture elongations hint to uniform deformation. Still, the influence of the sampling location and the small volumes of the APT data sets on the results should be kept in mind. Further, the migration of Mg vacancy complexes or MgSiCu/MgZnCu clusters can differ significantly from volume diffusion of individual Mg atoms.

The behavior of the material is determined by the complex dislocation-precipitation interaction during plastic deformation [19, 39]. In this study, however, clusters rather than precipitates predominate. A high fraction of solute atoms is incorporated into clusters, which are formed during plastic deformation. Vacancies, which are required by solutes to migrate [7], are produced in excess during deformation. As shown in the model above, their concentration is several orders of magnitude higher than the initial vacancy concentration after PA treatment, which is sufficient to achieve the required diffusion distances even at RT. The dislocations themselves may also contribute to enhanced diffusion along their core. However, a simple calculation of the contribution of pipe diffusion shows that it is one order of magnitude lower than the effect of excess vacancies.

It must further be noted that the dissolved Mg strongly contributes to

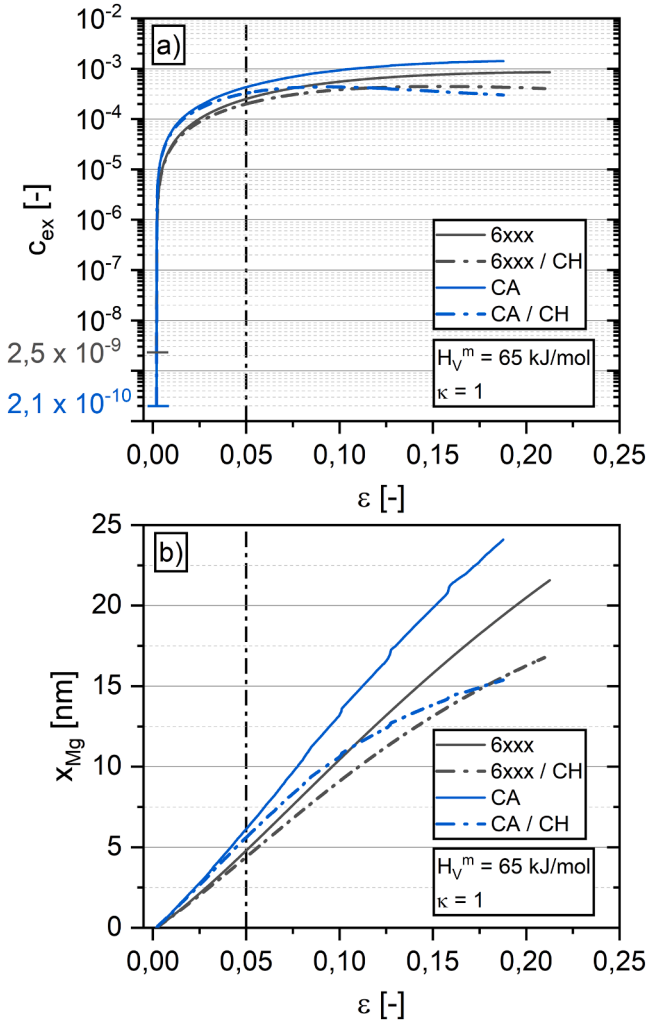

Fig. 3. Evolution of the excess vacancies (a) and diffusion length (b) during deformation. The black dashed lines mark the results at 5% strain. The gray and blue dashed lines illustrate the results when cluster hardening (CH) is considered.

the inhibition of the dislocation movement. The fact that clustering removes Mg atoms from the solution must therefore be taken into consideration. As reported in [40], an increase in Mg content results in a moderate effect on yield strength, but a strong effect on strain hardening behavior. Our calculations show that the contribution of clustering to the deformed state is about 45% in the case of the 6xxx alloy and roughly 30% for the crossover alloy. Compared to the AQ treated sample, whose yield strength results from solid solution strengthening, the PA-treated specimen demonstrates higher yield strength due to cluster hardening of 80 MPa for the 6xxx and 110 MPa for the CA alloy (Note that this is to be understood as net hardening, i.e. the hardening contribution of the clusters super-positioned with the loss of solid solution hardening due to the dilution of the matrix of alloying atoms by the cluster formation).

We may thus conclude that in the 6xxx series and crossover alloys studied, excess vacancies during plastic deformation significantly support the formation and growth of clusters, increasing their number density and volume fraction. This is somewhat comparable to the effect of intense cyclic plastic straining, which was deployed to form a dense distribution of clusters in [41]. In contrast to the increase in number density and cluster-volume fraction during deformation shown here, the study by Zhang et al. [11] did not find an increased number density of clusters in different strain states compared to the undeformed sample. It should be mentioned that their investigations were carried out on a different class of alloys under naturally aged conditions [11], and a comparison is therefore difficult. However, the contribution of newly formed clusters to strength itself can be seen as hypothetical non-dislocation-based strain hardening and must be considered when discussing the high strain hardening capacity of dense cluster structures.

In summary, the mechanism of strain-induced clustering observed in the pre-aged 6xxx and the crossover alloy in this study shows potential in the future optimization of the strength/formability tradeoff. Excess vacancies created by deformation support the formation of new clusters and thus increase their number density and the volume fraction of clusters. Extensive elongation potential and pronounced strain hardening capacity may be regarded as typical of cluster-hardened alloys.

Data availability

The raw/processed data required to reproduce these findings cannot be shared at this time as the data also forms part of an ongoing study.

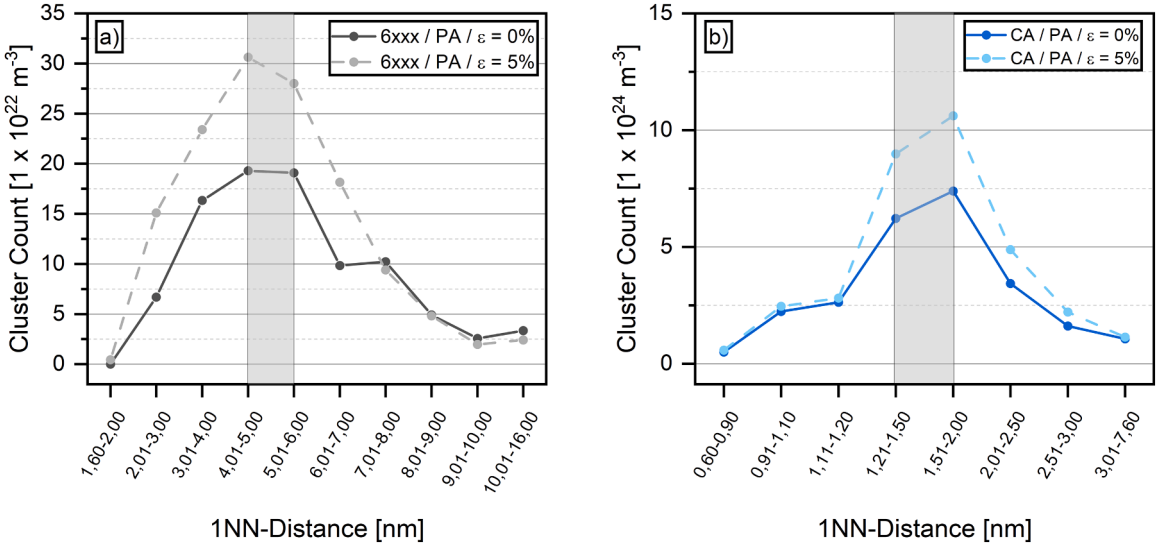

Fig. 4. Experimental distribution of the 1NN inter-cluster distance of (a) 6xxx alloy and (b) Crossover-Alloy defined by the Mg-based centroid. The gray and blue dashed lines represent the deformed state.

CRediT authorship contribution statement

Philip Aster: Conceptualization, Methodology, Investigation, Visualization, Writing – original draft. **Phillip Dumitraschkewitz:** Investigation, Writing – review & editing. **Peter J. Uggowitzer:** Conceptualization, Supervision, Writing – review & editing. **Florian Schmid:** Writing – review & editing. **Georg Falkinger:** Investigation, Writing – review & editing. **Katharina Strobel:** Writing – review & editing. **Peter Kutlesa:** Investigation. **Michael Tkadletz:** Investigation. **Stefan Pogatscher:** Project administration, Conceptualization, Supervision, Writing – review & editing.

Declaration of Competing Interest

The authors declare that they have no known competing financial interests or personal relationships that could have appeared to influence the work reported in this paper.

Acknowledgments

This work was funded by the Christian Doppler Research Association within the framework of the Christian Doppler Laboratory for Advanced Aluminum Alloys. Financial support from the Austrian Federal Ministry for Digital and Economic Affairs, the National Foundation for Research, Technology and Development and the Christian Doppler Research Association is gratefully acknowledged. The authors wish to express their sincere thanks to AMAG Rolling for the valuable discussions. We also thank Maximilian Schiester for his support in conducting the APT measurements.

References

[1] J. Peng, et al., Solute-vacancy clustering in aluminum, Acta Mater. 196 (2020) 747–758.
[2] S. Pogatscher, et al., Mechanisms controlling the artificial aging of Al–Mg–Si Alloys, Acta Mater. 59 (2011) 3352–3363.
[3] L. Stemper, et al., Giant Hardening Response in AlMgZn(Cu) alloys, Acta Mater. 206 (2021), 116617.
[4] P. Dumitraschkewitz, et al., Clustering in Age-Hardenable Aluminum Alloys, Adv. Eng. Mater. 20 (2018) online proceedings.
[5] M. Torsæter, et al., The influence of composition and natural aging on clustering during preaging in Al–Mg–Si alloys, J. Appl. Phys. 108 (2010) 73527.
[6] M. Werinos, et al., Hardening of Al–Mg–Si alloys: effect of trace elements and prolonged natural aging, Mater. Des. 107 (2016) 257–268.
[7] J.D. Robson, Deformation Enhanced Diffusion in Aluminium Alloys, Metall. Mater. Trans. A 51 (2020) 5401–5413.
[8] F. Schmid, et al., Enhanced aging kinetics in Al-Mg-Si alloys by up-quenching, Commun. Mater. 2 (2021) 1–12.
[9] A. Deschamps, et al., Low-temperature dynamic precipitation in a supersaturated AI-Zn-Mg alloy and related strain hardening, Philos. Mag. A 79 (1999) 2485–2504.
[10] M. Bignon, et al., Interactions between plastic deformation and precipitation in Aluminium alloys: a crystal plasticity model, Acta Mater. 247 (2023), 118735.
[11] P. Zhang, et al., Solute cluster evolution during deformation and high strain hardening capability in naturally aged Al–Zn–Mg alloy, Acta Mater. 207 (2021), 116682.
[12] L. Stemper, et al., On the potential of aluminum crossover alloys, Prog. Mater Sci. 124 (2022), 100873.
[13] P. Dumitraschkewitz, et al., Size-dependent diffusion controls natural aging in aluminium alloys, Nat. Commun. 10 (2019) 1–6.
[14] J.D. Gardiner, J. Behnsen, C.A. Brassey, Alpha shapes: determining 3D shape complexity across morphologically diverse structures, BMC Evol. Biol. 18 (2018) 184.
[15] T.L. Martin, et al., Comparing the consistency of atom probe tomography measurements of small-scale segregation and clustering between the LEAP 3000 and LEAP 5000 instruments, Microsc. Microanal.: Off. J. Microsc. Soc. America, Microbeam Anal. Soc., Microsc. Soc. Canada 23 (2017) 227–237.
[16] A.B. Spierings, et al., Microstructure characterization of SLM-processed Al-Mg-Sc-Zr alloy in the heat treated and HIPed condition, Addit. Manuf. 20 (2018) 173–181.
[17] A.V. Ceguerra, et al., A three-dimensional Markov field approach for the analysis of atomic clustering in atom probe data, Philos. Mag. 90 (2010) 1657–1683.
[18] C.R. Hutchinson, et al., Quantitative measurements of dynamic precipitation during fatigue of an Al–Zn–Mg–(Cu) alloy using small-angle X-ray scattering, Acta Mater. 74 (2014) 96–109.
[19] A. Deschamps, et al., In situ evaluation of dynamic precipitation during plastic straining of an Al–Zn–Mg–Cu alloy, Acta Mater. 60 (2012) 1905–1916.
[20] W. Sun, et al., Precipitation strengthening of aluminum alloys by room-temperature cyclic plasticity, Science 363 (2019) 972–975.
[21] Y. Lang, et al., Effect of strain-induced precipitation on the low angle grain boundary in AA7050 aluminum alloy, Mater. Des. (1980-2015) 32 (2011) 4241–4246.
[22] M.A. Afifi, Y.C. Wang, T.G. Langdon, Effect of dynamic plastic deformation on the microstructure and mechanical properties of an Al–Zn–Mg alloy, Mater. Sci. Eng.: A 784 (2020), 139287.
[23] H. Mecking, Y. Estrin, The effect of vacancy generation on plastic deformation, Scr. Metall. 14 (1980) 815–819.
[24] G. Gottstein, et al., Stored energy of 78K tensile deformed copper crystals, Acta Metall. 23 (1975) 641–652.
[25] M. Militzer, W.P. Sun, J.J. Jonas, Modelling the effect of deformation-induced vacancies on segregation and precipitation, Acta Metall. Mater. 42 (1994) 133–141.
[26] A. Seeger, D. Wolf, H. Mehrer, Analysis of tracer and nuclear magnetic resonance measurements of self-diffusion in aluminium, Phys. Status Solidi 48 (1971) 481–496.
[27] J.N. Mundy, Diffusion mechanism in F.C.C. metals, Phys. Status Solidi 144 (1987) 233–241.
[28] A. Falahati, P. Lang, E. Kozeschnik, Precipitation in Al-Alloy 6016 – The Role of Excess Vacancies, Mater. Sci. Forum 706-709 (2012) 317–322.
[29] P. Shewmon, Diffusion in solids. The Minerals, Metals & Materials Series, Springer International Publishing, Cham, 2016 s.l.
[30] K. Detemple, et al., In situ nuclear magnetic resonance investigation of deformation-generated vacancies in aluminum, Phys. Rev. B, Condens. Matter 52 (1995) 125–133.
[31] J. Bass, The formation and motion energies of vacancies in aluminium, Philos. Mag. 15 (1967) 717–730.
[32] S. Nenno, J.W. Kauffman, Detection of equilibrium vacancy concentrations in aluminium, Philos. Mag. 4 (1959) 1382–1384.
[33] P. Tzanetakis, J. Hillairet, G. Revel, The formation energy of vacancies in aluminium and magnesium, Phys. Status Solidi 75 (1976) 433–439.
[34] J. Embury, R. Nicholson, The nucleation of precipitates: the system Al-Zn-Mg, Acta Metall. 13 (1965) 403–417.
[35] S. Fujikawa, K. Hirano, Diffusion of 28Mg in aluminum, Mater. Sci. Eng. 27 (1977) 25–33.
[36] G. Gottstein, Materialwissenschaft Und Werkstofftechnik, Springer Berlin Heidelberg, Berlin, Heidelberg, 2014.
[37] L.M. Cheng, et al., The influence of precipitation on the work-hardening behavior of the aluminum alloys AA6111 and AA7030, Metall. Mater. Trans. A 34 (2003) 2473–2481.
[38] A.A. Csontos, E.A. Starke, The effect of inhomogeneous plastic deformation on the ductility and fracture behavior of age hardenable aluminum alloys, Int. J. Plast. 21 (2005) 1097–1118.
[39] F. Lu, et al., An improved modelling framework for strength and work hardening of precipitate strengthened Al–Mg–Si alloys, Mater. Sci. Eng.: A 832 (2022), 142500.
[40] Ø. Ryen, et al., Strengthening mechanisms in solid solution aluminum alloys, Metall. Mater. Trans. A 37 (2006) 1999–2006.
[41] L. Shi, et al., The effect of chemical patterning induced by cyclic plasticity on the formation of precipitates during aging of an Al–Mg–Si alloy, Mater. Sci. Eng.: A 815 (2021), 141265.